Original Article

Li Zhang, Mingwei Gao, Yueguang Wu, Huijuan Liu, Xuehan Zhuang, Yan Zhou, Qiqin Song, Shanshan Bi, Weimin Zhang* and Yongping Cui*

MST1 interactomes profiling across cell death in esophageal squamous cell carcinoma

https://doi.org/10.1515/mr-2024-0031
Received March 30, 2024; accepted May 27, 2024;
published online June 14, 2024

Abstract

Objectives: Resistance to apoptosis in esophageal squamous cell carcinoma (ESCC) constitutes a significant impediment to treatment efficacy. Exploring alternative cell death pathways and their regulatory factors beyond apoptosis is crucial for overcoming drug resistance and enhancing therapeutic outcomes in ESCC.

Methods: Mammalian Ste 20-like kinase 1 (MST1) is implicated in regulating various cell deaths, including apoptosis, autophagy, and pyroptosis. Employing enhanced ascorbate peroxidase 2 (APEX2) proximity labeling coupled with immunoprecipitation-mass spectrometry (IP-MS), we elucidated the interactomes of MST1 across these three cell death paradigms.

Results: Proteomic profiling unveiled the functional roles and subcellular localization of MST1 and its interacting proteins during normal proliferation and various cell death processes. Notably, MST1 exhibited an expanded interactome during cell death compared to normal proliferation and chromosome remodeling functions consistently. In apoptosis, there was a notable increase of mitosis-associated proteins such as INCENP, ANLN, KIF23, SHCBP1 and SUPT16H, which interacted with MST1, alongside decreased expression of the pre-apoptotic protein STK3. During autophagy, the bindings of DNA repair-related proteins CBX8 and m^6A reader YTHDC1 to MST1 were enhanced. In pyroptosis, LRRFIP2 and FLII which can inhibit pyroptosis increasingly binding to MST1.

Conclusions: Our findings delineate potential mechanisms through which MST1 and its interactomes regulate cell death, paving the way for further investigation to validate and consolidate these observations.

Keywords: MST1; cell death; ESCC; proteomics; APEX2

Introduction

Esophageal cancer ranks among the most prevalent malignant tumors globally and stands as the sixth leading cause of cancer-related mortality [1]. Resistance to apoptosis in esophageal squamous cell carcinoma (ESCC) constitutes a significant contributor to treatment failure [2]. Therefore, exploring alternative cell death pathways and their regulatory factor beyond apoptosis holds paramount importance in overcoming drug resistance and enhancing therapeutic outcomes in ESCC. In recent years, there has been a growing focus on the involvement of Mammalian Ste 20-like kinase 1 (MST1) in cell death regulations. For instance, MST1 has been implicated in suppressing the progression of pancreatic ductal adenocarcinoma (PDAC) cells, partly through ROS-induced pyroptosis [3]. Additionally, Wilkinson et al. demonstrated that MST1/2 phosphorylation of LC3, a pivotal molecule in the autophagy process, is crucial for autophagy induction [4].

MST1, a mammalian counterpart of the Hippo signaling pathway, serves as a crucial regulator in stem cell self-renewal, tissue regeneration, and organ size control [5–7]. This pathway involves a kinase cascade consisting of MST1/2, the scaffolding protein Salvador/WW45 (Sav), the nuclear Dbf2–related family kinases LATS1 and LATS2 (LATS1/2), and the adaptor protein MOB1. MST1/2 phosphorylates and activates LATS1/2–MOB1, leading to the phosphorylation of Yes-associated protein/transcriptional coactivator with PDZ-binding motif (YAP/TAZ) [8, 9]. Phosphorylated YAP/TAZ

***Corresponding authors: Weimin Zhang and Yongping Cui**, Cancer Institute, Shenzhen-Peking University-the Hong Kong University of Science and Technology Medical Center, Shenzhen, Guangdong 518035, China, E-mail: zhangweimin@bjmu.edu.cn (W. Zhang), cuiyp@sphmc.org (Y. Cui). https://orcid.org/0000-0002-5961-4125 (Y. Cui)
Li Zhang, Yueguang Wu, Xuehan Zhuang, Qiqin Song and Shanshan Bi, Cancer Institute, Shenzhen-Peking University-the Hong Kong University of Science and Technology Medical Center, Shenzhen, Guangdong, China
Mingwei Gao, Department of Oncology, Peking University Shenzhen Hospital, Shenzhen, Guangdong, China
Huijuan Liu and Yan Zhou, Institute of Cancer Research, Shenzhen Bay Laboratory, Shenzhen, Guangdong, China

is either degraded or sequestered in the cytoplasm by the 14-3-3 protein. Upon activation of the Hippo pathway, YAP/TAZ translocates to the nucleus, where it interacts with the TEA domain transcription factor (TEAD) to promote the expression of pro-proliferative and pro-survival genes, facilitating cell proliferation [10, 11].

Pan-cancer expression analysis demonstrated esophageal squamous cell carcinomated significantly elevated levels of MST1 across seven different cancer types (Figure 1a). Specifically, analysis of 155 patients with revealed significant overexpression of MST1 in tumor tissues (Figure 1b). These findings imply potential aberrant activation of MST1 in tumor tissues, suggesting its candidacy as a therapeutic target for ESCC. Nevertheless, the functional role and regulatory impact of MST1 and its interactomes on cell death in ESCC remain inadequately understood.

This study aimed to investigate various forms of regulated cell death, encompassing apoptosis, autophagy, pyroptosis, as well as the common module representing fundamental functions of MST1 and its interactomes across different cell death. Our focus was specifically directed towards elucidating the regulatory role of MST1 and its interactomes (Figure 1c). Thus, we established cell death models including apoptosis, autophagy, and pyroptosis in ESCC cells. In these cell models, we used APEX2 proximity labeling technology combined with immunoprecipitation-

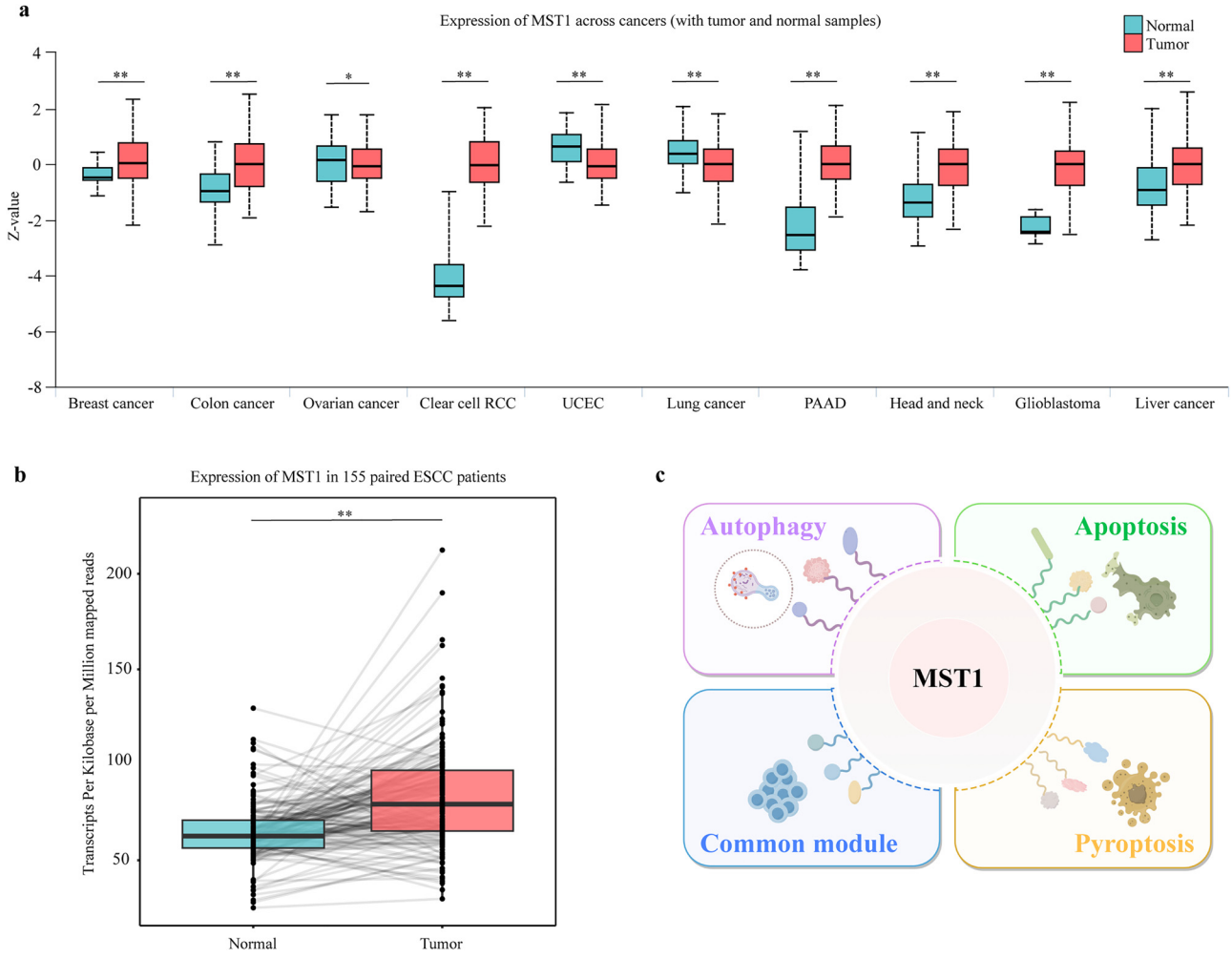

Figure 1: Expression of MST1 across cancers. (a) The expression of MST1 in different cancer species. MST1 was significantly overexpressed in seven cancers, which was analyzed and visualized using the UALCAN (ualcan.path.uab.edu) website. RCC, renal cell carcinoma; UCEC, uterine corpus endometrial carcinoma; PAAD, pancreatic adenocarcinoma (**p<0.01; *p<0.05). (b) The expression of MST1 in tumor tissues of 155 patients with esophageal squamous cell carcinoma was significantly higher than that in adjacent normal tissues (**p<0.01). The data generated by this paper is available through the genome sequence archive (GSA) in the BIG Data Center (http://bigd.big.ac.cn/gsa), Beijing Institute of Genomics (BIG), Chinese Academy of Sciences: HRA003107 (WGS & RNA-seq, https://ngdc.cncb.ac.cn/gsa-human/browse/HRA003107), HRA003533 (WGBS, https://ngdc.cncb.ac.cn/gsa-human/browse/HRA003533). (c) The schematic diagram of MST1 and its interactomes exhibit varied roles in apoptosis, autophagy, pyroptosis and the c.

mass spectrometry (IP-MS) to capture and identify the protein interactome of MST1. Through comprehensive proteomic analysis, we examined the influence of MST1 and its interacting proteins across different cell death conditions, constructing a protein interaction network map for MST1. These findings contribute to a deeper understanding of the potential mechanisms underlying MST1 in regulating cell death and lay a theoretical foundation for the development of innovative therapeutic approaches.

Materials and methods

Cell lines and reagents

The human ESCC cell lines KYSE150 were kindly supplied by Dr. Y. Shimada. ESCC cells were cultured in RPMI 1640 (GIBCO) medium supplemented with 10 % (v/v) fetal bovine serum (FBS) and 100 U/mL penicillin/streptomycin (GIBCO). All the cell lines were free of mycoplasma and maintained at 37 °C and 5 % CO_2. To ensure the reliability of the experimental results, the passage number of cells used in experiment was less than 10.

Cell viability assays

Cell proliferation was conducted with a Cell Counting Kit-8 (CCK8) assay (Vazyme Biotech). KYSE150 cells were seeded in 96-well plates (10,000 cells/well) and treated with gradient concentrations of DDP, rapamycin or TSA for 24 h. Then, 10 μL of CCK-8 solution was added to each well, and the plates were further incubated for 1 h at 37 °C according to the manufacturer's instructions. Optical density (OD) values were obtained at 450 nm using a microplate reader (BioTek, Winooski, VT, USA). Each experiment was conducted three times with six replicates. Drug treatment was added when the cell growth reached a confluence of 70–80 % to reduce the effect of cell density on the experiment.

Western blotting

The cells were digested with 0.25 % trypsin and collected. Protease inhibitors (Roche) and phosphatase inhibitors (Roche) were added to the cell lysates, which were incubated on ice for 30 min. Then, the samples were centrifuged at 15,000×*g* and 4 °C for 15 min, after which the supernatant was collected. The protein concentration was detected with a BCA kit (Beyotime). Fifty micrograms of each sample were separated on a 10 % SDS-PAGE gel, transferred to a PVDF membrane, blocked with 5 % non-fat milk at room temperature for 2 h, incubated at 4 °C overnight with primary antibody at room temperature for 1 h with secondary antibody, and incubated with an enhanced chemiluminescence kit (ECL) (YEASEN) for 1 min. A ChemiDoc XRS$^+$ System (BOLE/Bio-Rad) was used for imaging.

Immunofluorescence

Paraformaldehyde-fixed KYSE150 cells cultured on coverslips were permeabilized with PBS containing 0.3 % Triton, 10 % FBS and 1 % BSA at RT for 1 h and then incubated with the indicated primary antibody at 4 °C overnight. The cells were then washed with PBS 3 times, incubated with secondary antibody for 2 h, and washed with PBS 3 times, followed by the addition of the antifade reagent DAPI (Invitrogen) to each coverslip. Images were acquired using a Zeiss LSM 980 confocal laser scanning microscope.

For the Cyto-ID immunofluorescence staining procedures, the CYTO-ID® Autophagy Detection Kit (Enzo Life Sciences) manual was used.

Construction of the APEX2-MST1 plasmid

Forward primer (CGGAAGTGGAAGCGGCGTCGACATGGAGACGGTACAGCTGAGGAA) and reverse primer (CTTTGTAGTCCATGGTACGCGTGAAGTTTTGTTGCCGTCTCTTCTTAGC) were used to amplify the CDS of human MST1 by PCR from NE2 (normal esophageal cells) by PCR, and the ERM-APEX2 plasmid (Addgene, 79,055) was also amplified using PrimeSTAR HS high-fidelity PCR enzyme (TaKaRa).

The ClonExpress® Ultra One Step Cloning Kit (Vazyme Biotech) was used to clone the PCR products between the SalI and MluI cleavage sites on the ERM-APEX2 plasmid, and Sangon verification was used to confirm the DNA sequence of the constructed plasmid.

In situ labeling of MST1-interacting proteins

Lipofectamine™ 3,000 transfection reagent (Thermo Fisher) was used to introduce the constructed APEX2-MST1 expression plasmid into ESCC cells, and cell lines with stable expression of the APEX2-MST1 fusion protein were obtained through puromycin selection. After drug treatment, the cells stably expressing APEX2-MST1 were incubated with 500 μmol/L of biotinylated tyramide (MedChemExpress) at

37 °C for 30 min, after which H2O2 at a final concentration of 1 mmol/L was added, and the cells were incubated for 1 min. The reaction was quenched by adding a final concentration of 5 mmol/L Trolox (MedChemExpress) and 10 mmol/L sodium ascorbate (MedChemExpress). The cells were washed 3 times with a quencher solution containing 5 mmol/L Trolox and 10 mmol/L sodium ascorbate and fixed with 4 % paraformaldehyde for immunofluorescence or lysed with a Dynabeads MyOne streptomycin avidin C1 magnetic bead (Invitrogen) for affinity capture.

Affinity capture of biotinylated proteins

ESCC cells were washed twice with quencher solution and lysed in 200 µL of ice-cold RIPA lysis buffer supplemented with 25 mmol/L Tris (pH 7.5), 150 mmol/L NaCl, 1 % Triton X-100, 0.16 % sodium deoxycholate, 0.16 % SDS, 1.5 mmol/L EDTA, 5 mmol/L Trolox, 10 mmol/L L-ascorbate and protease inhibitors (cOmplete, Roche, Basel, Switzerland). The cell suspensions were centrifuged for 15 min at 14,000×*g* and 4 °C, after which the total protein concentration was quantified with a Pierce 660 nm spectrophotometer (Thermo Scientific). Streptavidin magnetic beads (Invitrogen) were equilibrated with RIPA lysis buffer twice. Each lysate was incubated with 50 µL of bead slurry in microcentrifuge tubes with rotation at 4 °C overnight. The beads underwent a series of washes: twice with 1 mL of RIPA lysis buffer, followed by a single wash with 1 mL of 1 mol/L KCl, another single wash with 1 mL of 100 mmol/L sodium carbonate, then twice with 1 mL of 2 mol/L urea, and finally, two more washes with 1 mL of RIPA lysis buffer.

Immunoprecipitation

IP beads were washed twice with NT-2 buffer and supernatant aspirated using a magnetic rack. Subsequently, 100 µL of NT-2 buffer containing 50 mmol/L Tris-HCl (pH7.5), 150 mmol/L NaCl, 2 mmol/L EDTA, 1 % NP40 and 2 µg of antibody (or manufacturer's recommended amount) were added, followed by 1-h incubation at 4 °C on a rotator. Cells were digested, washed, and centrifuged into a 1.5 mL EP tube. NP-40 lysis buffer with protease and phosphatase inhibitors was added, vigorously shaken, and incubated on ice with intermittent shaking for 30 min. A low-temperature high-speed centrifuge was preset to 4 °C. Centrifugation was conducted at 12,000 g for 10 min at 4 °C, and the supernatant was transferred to a fresh 1.5 mL EP tube. A 10 µL aliquot of the supernatant was mixed with 40 µL of NP-40 lysis buffer and 12.5 µL of loading buffer (input), boiled at 100 °C for 10 min, and stored at −20 °C. The supernatant was aspirated from the EP tube using a magnetic rack, and the beads were washed three times with NT-2 buffer. Protein lysis buffer was added to reach a volume of 250 µL, and the mixture was incubated overnight at 4 °C on a rotator. After incubation, the beads were washed five times with NT-2 buffer and mixed with 30 µL of NP-40 lysis buffer and 7.5 µL of loading buffer. The mixture was boiled at 100 °C for 10 min and stored at −20 °C.

Trypsin digestion of resin-bound proteins

Three biologically independent labeling experiments were conducted for each condition and three replicates were merged.

Resuspend resins in 50 µL Elution buffer I which contains 50 mmol/L Tris-HCl (pH=8.0), 2 mol/L urea, 10 µg/mL Sequencing Grade Trypsin; 1 mmol/L DTT. Incubate in a thermomixer at 30 °C at 400 rpm for 60 min. Centrifuge at 2,500×*g* for 2 min at 4 °C. Transfer supernatant to a fresh vial (label "digest I", most target proteins and its binding proteins are released from the beads to the supernatant). Resuspend the pelleted beads in 25 µL Elution buffer II which contains 50 mM Tris-HCl (pH=8.0), 2 mol/L urea, and 5 mmol/L IAA. Protect from light. Centrifuge at 2,500×*g* for 2 min at 4 °C, collect the supernatant (more target proteins and its binding proteins are washed in to the supernatant). The supernatant was combined with the previous "digest I". Protect from light. This process was repeated once. All the above supernatants were combined, and another 250 ng of sequencing trypsin was added to the combined supernatant, which was subsequently digested in a thermomixer at 32 °C at 600 rpm overnight. Protect samples from light.

Preparation by digestion for mass spectrometry analysis: the reaction was stopped by adding 10 % formic acid to the reaction mixture at a v:v ratio of 1:25.

The samples were desalted using a Pierce C^{18} spin column (Thermo Fisher) and subjected to MS.

Liquid chromatography-tandem mass spectrometry

MS/MS was conducted on a Q-Exactive Orbitrap mass spectrometer (Thermo Finnigan, Bremen, Germany) for peptide analysis. The elution of peptides was achieved using a

240-min gradient, ranging from 2 % to 33 % (B). The transition of peptides into the gaseous phase was facilitated by positive ion electrospray ionization at a voltage of 2.5 kV. In each MS survey scan, the top 10 most abundant multiply charged precursor ions, with *m*/*z* ratios between 300 and 2,200 and an intensity threshold of 500, were selected using an FT mass resolution of 70,000. These ions were then fragmented using HCD, and the resulting tandem mass spectra were acquired with an FT resolution of 35,000. A normalized collision energy of 33 was applied, and previously targeted precursors were dynamically excluded from further isolation and activation for 30 s, with a mass tolerance of 5 ppm.

MS data processing

Files were analyzed with the Proteome Discoverer 2.5 software package (Thermo Finnigan, Thermo Fisher) using the Sequest search engine and the UniProt human (*Homo sapiens*) database.

The search was conducted using cysteine carbamidomethylation as a static modification and methionine oxidation as a dynamic modification. We removed keratin and some ribosomal proteins, which are usually regarded as contaminated proteins. Two missed cleavage sites were permitted, along with a precursor mass tolerance of 10 ppm and a fragment mass tolerance of 0.05 Da. False discovery rate (FDR) validation was set to <0.01 and unique peptides ≥1.

Gene Ontology analysis and visualization

Gene ontology (GO) 'cellular component' analysis were performed using the WebGestalt 2019 gene set analysis toolkit with an FDR <0.05 [49]. The *H. sapiens* genome protein-coding database was used as a reference. The elements in summary of proteins and their associated molecular functions binding to MST1 were from www.Figdraw.com.

To visualize the nonredundant biological terms in a functionally grouped network, the Cytoscape plugin ClueGo 3.10.1 was used [50]. The ClueGO network was created with kappa statistics and reflects the relationships between the terms based on the similarity of their associated genes with a kappa score of 0.4. The node color is switched between functional groups and cluster distribution on the network. Related terms that shared similar associated genes were fused to reduce redundancy.

Results

Induction of apoptosis, autophagy, and pyroptosis in ESCC cell lines

We hypothesized that MST1 plays a role in regulating different forms of cell death by binding to different proteins. Therefore, this study will test this hypothesis by analyzing the protein interactomes in different cell death models. To establish cell death models, we determined the half-maximal inhibitory concentration (IC50) values of four drugs known to induce cell death in ESCC, selected based on their mechanisms of action and potential therapeutic relevance. We assessed the expression and phosphorylation status of MST1 and its associated components within the Hippo pathway (Figure 2a). Our results indicated decreased expression and phosphorylation of MST1 following induction with the selected drugs.

Induction of apoptosis in ESCC cells by cisplatin

Apoptosis is a highly regulated form of cell death that plays a critical role in cancer development and treatment [12]. We examined the induction of apoptosis in ESCC cells using cisplatin (also called DDP), a commonly used chemotherapeutic agent known to trigger apoptotic pathways [13, 14]. Caspases are a set of proteases in the cytoplasm called aspartic acid with cysteine proteolytic enzymes [15]. In the absence of upstream signals, the caspase family in the activation of the enzyme to the original form exists in the cytoplasm. Only when self-cleaving activation occurs in response to upstream signals can substrate recognition and cutting be performed, and then apoptosis can be initiated.

Twenty-four hours post-treatment of KYSE150 cells with 30 μmol/L DDP, we detected up-regulated protein expression levels of caspase-3, caspase-7, caspase-9, and their cleavage forms (Figure 2b), indicating activation of the caspase family and promotion of apoptosis following cisplatin induction.

Induction of pyroptosis in ESCC cells by TSA

Pyroptosis is an inflammatory form of programmed cell death that is often associated with immune responses [16]. We investigated the induction of pyroptosis in ESCC cells using trichostatin A (TSA), a histone deacetylase HDAC inhibitor known to activate pyroptotic pathways [17]. Elevated HDAC1 expression in ESCC tissues correlates significantly with higher lymph node metastasis and TNM stage. HDAC inhibitors have demonstrated potent anti-ESCC

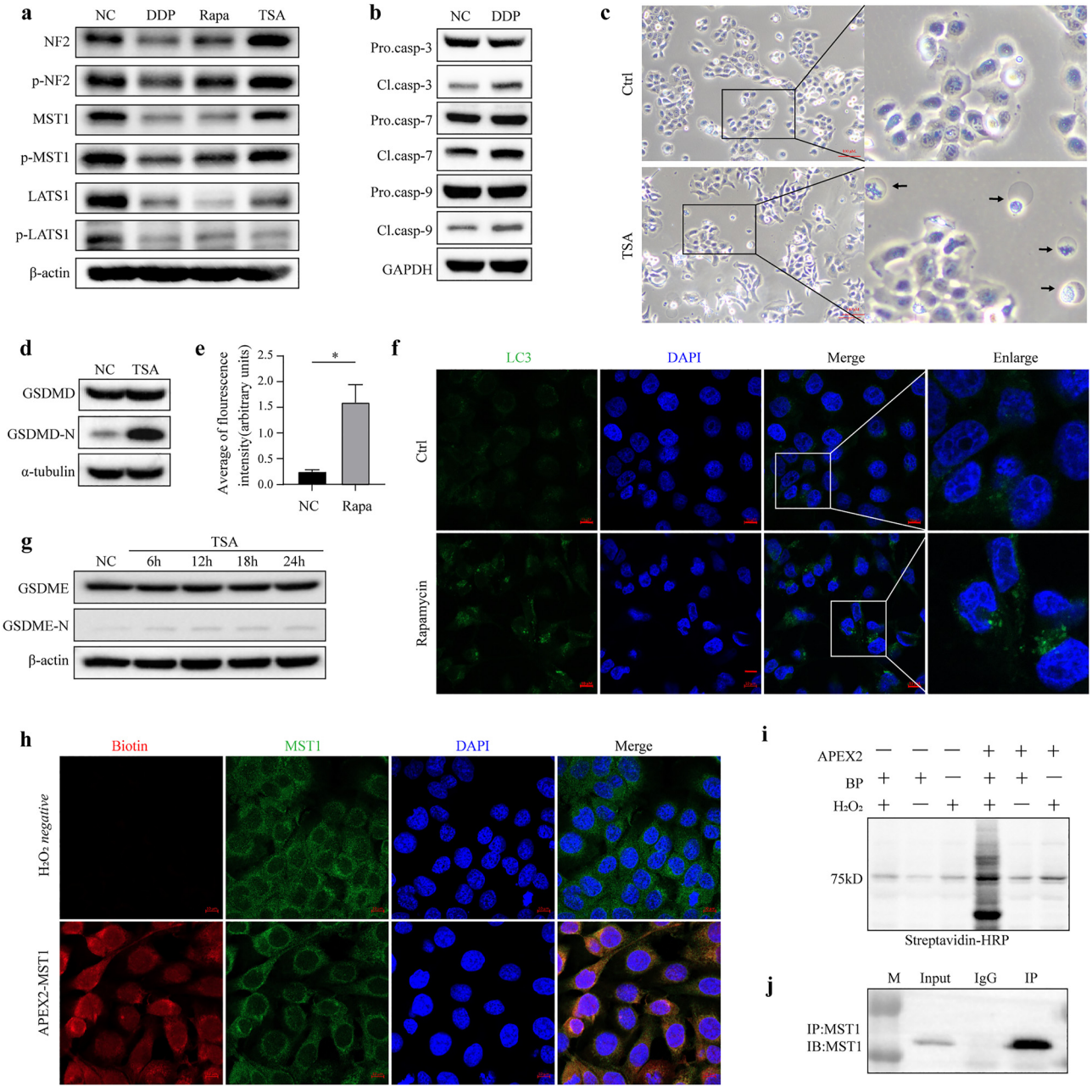

Figure 2: Induction of cell death in ESCC cells. (a) MST1 expression and phosphorylation decreased after 24 h of treatment with DDP, rapamycin, or TSA in KYSE150 cells. (b) Cleavage of Caspase-3, Caspase-7, and Caspase-9 in KYSE150 cells significantly increased after 24-h treatment with 35 μmol/L DDP. (c) Morphological features indicative of pyroptosis, including cell swelling and plasma membrane bubbling, were observed in cells 24 h after treatment with 1 μmol/L TSA. (d) Cleavage of GSDMD increased in cells following 24-h induction with 1 μmol/L TSA. (e) and (f) LC3 expression significantly increased in KYSE150 cells following treatment with 10 μmol/L rapamycin for 24 h (*$p<0.05$). (g) Cleavage of GSDME increased in cells following 24-h induction with 1 μmol/L TSA. (h) Immunofluorescence-validated APEX2-MST1 labeling specificity in KYSE150 cells, biotin red, MST1 green; right: expression of the APEX2-MST1 fusion protein. APEX2, ascorbate peroxidase 2. (i) Streptavidin-HRP Western blotting of induced protein biotinylation in lysates from cells expressing APEX2-MST1. BP, biotin-phenol. (j) The IP efficiency was verified by Western blotting. IP, immunoprecipitation.

effects *in vivo*, with moderate inhibition of angiogenesis [18, 19]. Gasdermin family members, particularly GSDMD and GSDME, act as executors of pyroptosis, facilitating cell membrane perforation and pore formation [20].

Following induction with 1 μmol/L TSA for 24 h, we observed increased expression of cleaved GSDMD and GSDME (Figure 2d–g), accompanied by distinctive morphological changes in ESCC cells indicative of pyroptosis, including

cell swelling and extensive plasma membrane bubbling (Figure 2c). These findings suggest a significant enhancement of pyroptosis in ESCC cells following TSA treatment.

Induction of autophagy in ESCC cells by rapamycin

Autophagy is a cellular process involved in the degradation and recycling of cellular components and has both pro-survival and pro-death effects depending on the context [21, 22]. Rapamycin, an inhibitor of the mTOR pathway, serves as a positive control drug to induce and promote autophagy. In nude mice models, rapamycin alone or in combination with cisplatin inhibits the growth of ESCC [6, 23].

Following induction with 10 μmol/L rapamycin for 24 h, we assessed the expression and subcellular localization of LC3 using immunofluorescence in KYSE150 cells. Our results revealed a significant increase in LC3 expression (Figure 2e and f) with cytoplasmic concentration, indicating a substantial elevation in autophagy levels in ESCC cells.

Construction of the APEX2-MST1 fusion protein for proximity labeling

Proximity labeling is a method wherein a labeling enzyme fused to the protein of interest marks the protein's interaction network *in vivo*, facilitating subsequent *ex vivo* analysis [24]. In this study, a second-generation highly active ascorbate peroxidase (APEX2) was tethered to MST1 to enable proximity labeling. APEX2 utilizes hydrogen peroxide (H_2O_2) to catalyze the oxidation of a cell-permeable biotin-tyramide substrate, generating biotin phenoxyl radicals that label aromatic amino acids within approximately 20 nm of the enzyme. This technique allowed for the labeling and identification of all proteins proximal to MST1 under various inducing conditions via mass spectrometry.

To assess the expression and subcellular distribution of the APEX2-MST1 fusion protein, Western blotting and immunocytochemistry using antibodies against MST1 were performed (Figure 2h and i), confirming strong cytosolic localization of the fusion protein.

While proximity labeling offers the advantage of being performed in intact living cells, it is prone to high background levels. Therefore, we employed immunoprecipitation-mass spectrometry (IP-MS) to mitigate background noise (Figure 2j), intersecting the proteins identified by both techniques (Table S1–3).

Bioinformatic analysis of MST1 interactomes in different cell death

Biological process analysis of MST1 interactomes

In this study, we employed the intersection of proteins which were identified by APEX2 and IP-MS as the interacting proteins of MST1 in different cell death to increase the credibility of the results, which could effectively exclude non-specific binding proteins and non-directly binding proteins. Due to the sensitivity and accuracy of protein quantification, we have adopted the Fold change values detected by APEX2. Proteins that bind to MST1 across cross athree cell death with insignificant variations ($0.667 < \text{Fold change} > 1.500$) are designated as the common module, which serves to reflect the fundamental functions of MST1 and its interactomes. Regarding the proteins identified by APEX2 and IP-MS, MST1 exhibited twice or more interaction partners during cell death compared to the common module (Figure 3a). To visualize the functional networks associated with different cell death, we conducted biological process (BP) analysis using the ClueGo plugin in Cytoscape. Figure 3b–e illustrates the GO biological processes associated with MST1-interaction proteins in apoptosis, autophagy, and pyroptosis and the common module', respectively.

Notably, mitotic regulation (mitotic cell cycle regulation, mitotic DNA replication initiation and cytokinesis) was enriched in the apoptosis model (Figure 3b), and biological processes related to DNA repair and DNA morphological remodeling (DNA topological change, Chromatin assembly and Chromosome organization) were enriched in the autophagy model (Figure 3c). DNA structure change and cytoskeleton remodeling were observed in the pyroptosis model (Figure 3d). Collectively, these observations revealed that MST1 was likely involved in the chromosome remodeling during cell death.

In the common module, the biological processes of MST1 interactomes encompass not only well-established roles such as cytoplasmic translation, nucleic acid transport, and actin cytoskeletal organization, but also previously unreported regulations associated with telomere maintenance.

According to the afore mentioned analysis, the quantitative and functional distinctions among the proteomes obtained under the four conditions indicate MST1-interacting proteins demonstrate common molecular functionalities in different cell death, including chromatin remodeling and cytoskeletal reorganization. Nonetheless, they also possess distinct and unique functionalities, potentially associated to cellular responses to different death stimuli.

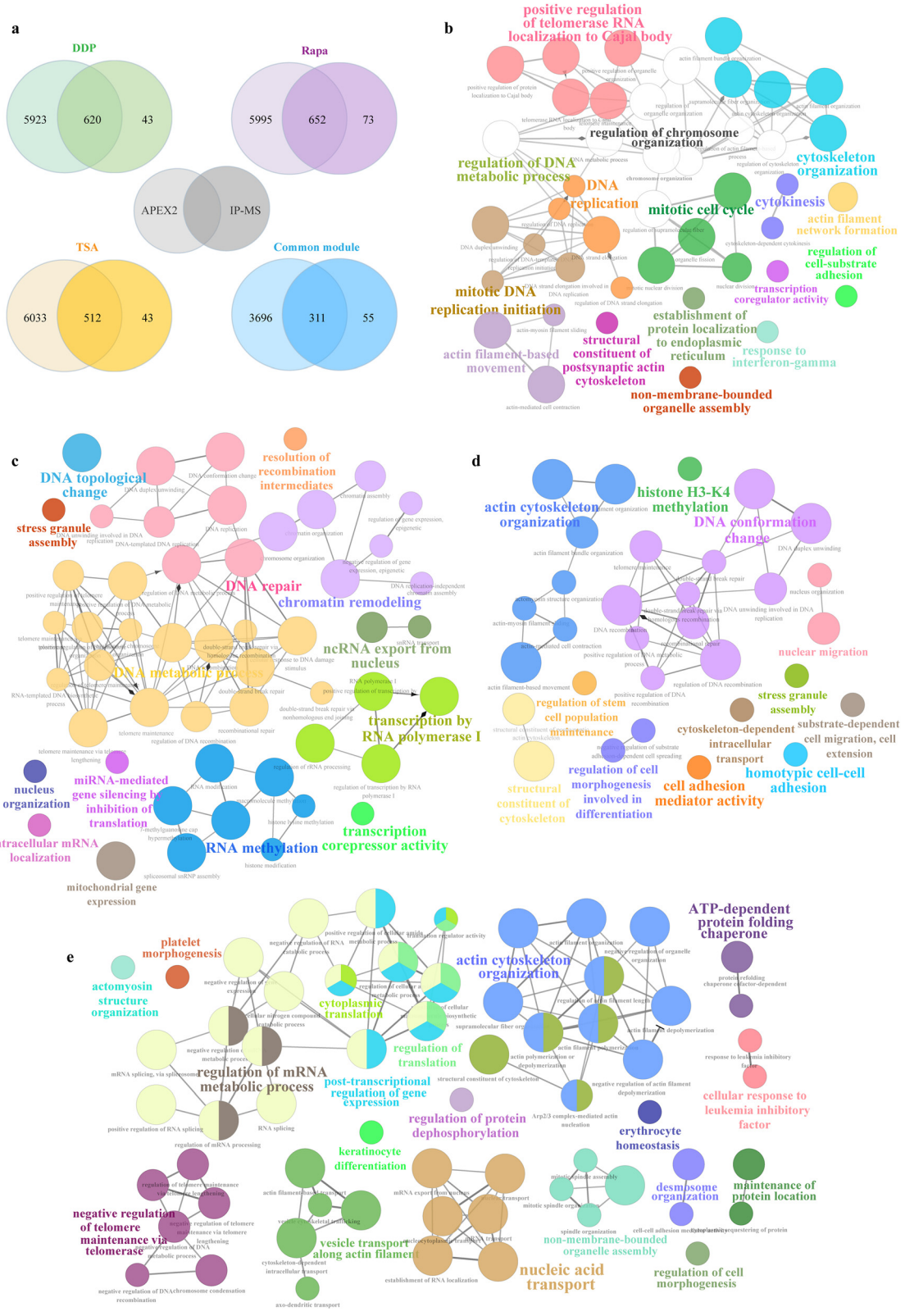

Figure 3: Proteomic analysis of MST1-interacting proteins. (a) Venn diagram illustrating the overlap between APEX2 and IP-MS capture of MST1-interacting proteins. Biological processes analysis of MST1-binding proteins in (b) apoptosis, (c) autophagy, (d) pyroptosis, and (e) the common module. Top enriched GO terms are depicted as nodes, with node size indicating term enrichment significance ($p<0.05$ for each GO term).

Proteins that significantly increase or decrease in binding to MST1

We screened the significantly increased and decreased proteins in the three death models based on their fold change (fold change ≤1.500 or≥0.667) and p-value ($p<0.05$) as depicted in Figure 4a–c, and identified several known MST1-binding proteins, including STK3 and PTPN14 (apoptosis), ACTB and MYO5A (autophagy), YBX1 and RASSF1 (pyroptosis), along with several candidate proteins that have not been directly shown to interact with MST1 and analyzed interactions between these screened proteins using STRING database (Figure 4d).

Proteins associated with mitosis and DNA replication, such as INCENP, ANLN, SUPT16H, SHCBP1 and KIF23 were significantly increased in the apoptosis model [25–29]. Proteins related to EMT and cell junction, including JUP and DSP, decreased [30, 31]. Notably, the binding of the pro-apoptotic kinase STK3 and PTPN14, the negative regulator of YAP to MST1 also decreased [32].

In the autophagy model, YTHDC1, an N6-methyladenosine (m^6A) reader, and CBX8, which is required for efficient DNA repair and chromosome remodeling, were significantly increased [33] together with the topoisomerases TOP3A and TOP2B. Most of the proteins binding to MST1 that decreased were cytoskeletal proteins, including MYO5A, MYO1B and ACTB.

Notably, the levels of LRRFIP2 and FLII increased in the pyroptosis model. The interaction between MST1 and NPM3, a crucial factor in chromatin remodeling [34],

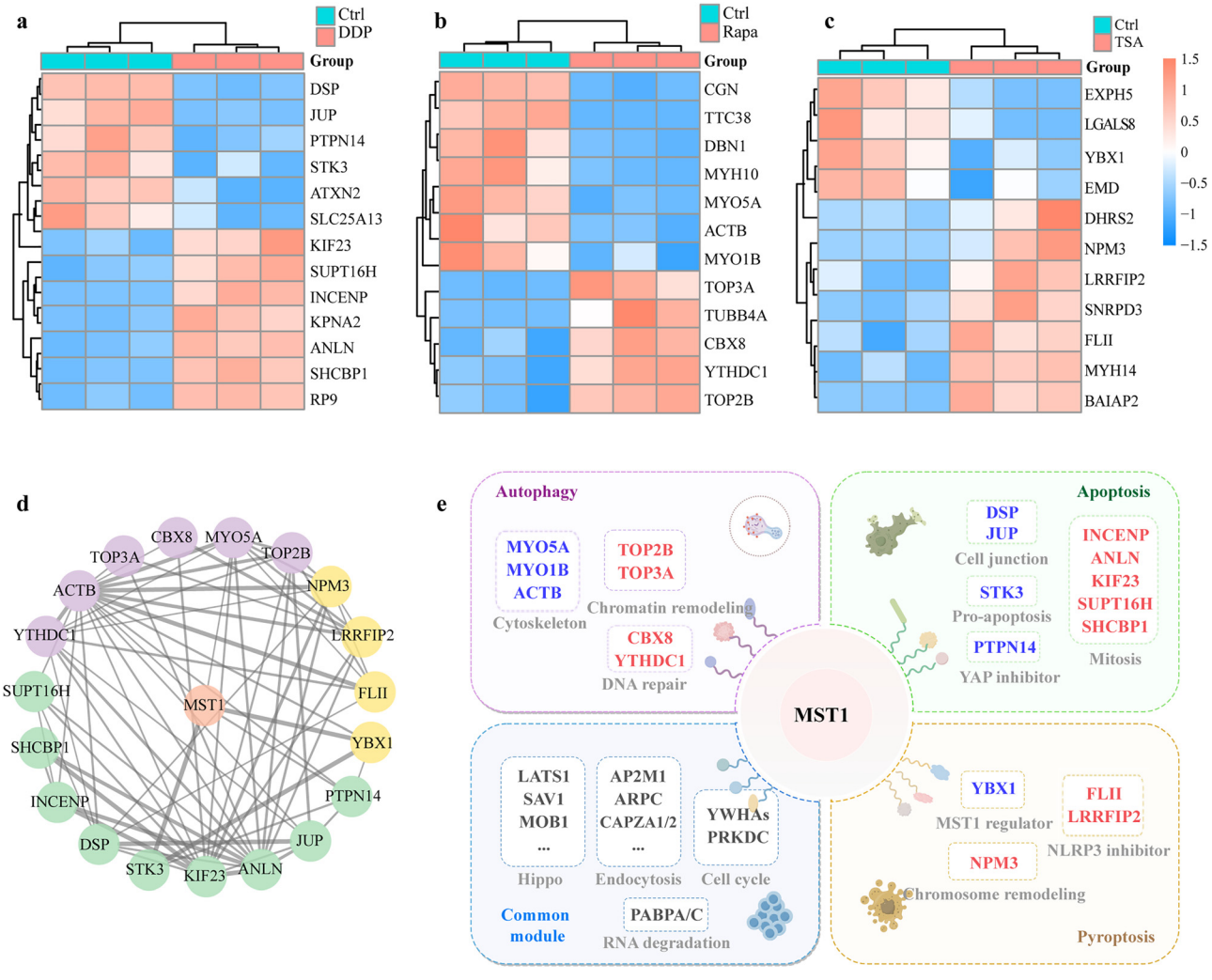

Figure 4: Identification of significantly increased and decreased interacting proteins of MST1 in different cell death. Identification of significantly increased and decreased interacting proteins of MST1 in (a) apoptosis, (b) autophagy and (c) pyroptosis. (d) Protein interaction networks based on STRING database in three death models (purple, autophagy; green, apoptosis and yellow, pyroptosis). (e) Summary of proteins and their associated molecular functions binding to MST1 during various cell death processes. Blue indicates significantly decreased proteins, red indicates significantly increased proteins, and gray represents the molecular functions of these proteins.

significantly increased. While chromatin remodeling was not enriched in the BP analysis in the pyroptosis model, the notable elevation of NPM3 hints at a possible involvement of MST1 in facilitating chromatin remodeling during pyroptosis, echoing the biological processes associated with MST1-interacting proteins in apoptosis and autophagy. Additionally, the abundance of YBX1, a DNA- and RNA-binding protein that can regulate MST1 upstream [35], was significantly downregulated.

In the common module, MST1 interactomes are mainly divided into the following parts, suggesting the basic functions of MST1: proteins related to the Hippo pathway, such as LATS1, SAV1, MOB1, and STK3; proteins related to cell cycle regulation, such as YWHA family proteins and PRKDC [36]; endocytosis-related proteins ARPC3/4, CAPZA1/2, and AP2A1/AP2M1 [37]; and PABPC1/4, related to RNA degradation [38]. Interestingly, the autophagy substrate SQSTM1 is also among these proteins (Table S1).

Cell component analysis of MST1 interactomes in different cell death

The subcellular localization of MST1-binding proteins in different cell death models partially corresponds to the BP analysis mentioned above. We utilized the WebGestalt analysis toolkit to elucidate the subcellular localization of the MST1-interacting proteome (Figure 5a–d). In the common module, MST1 partners were found distributed across the cytoplasm, cell-substrate junctions, replication forks, and chromosomal regions, with similar distributions observed in both the apoptosis and pyroptosis models. However, in the apoptosis model, MST1-binding proteins were uniquely localized to the midbody and exoribonuclease, while in the autophagy model, proteins were primarily found in nuclear speckles, the small nuclear ribonucleoprotein complex, and the methyltransferase complex. In the pyroptosis model, some proteins exhibited unique

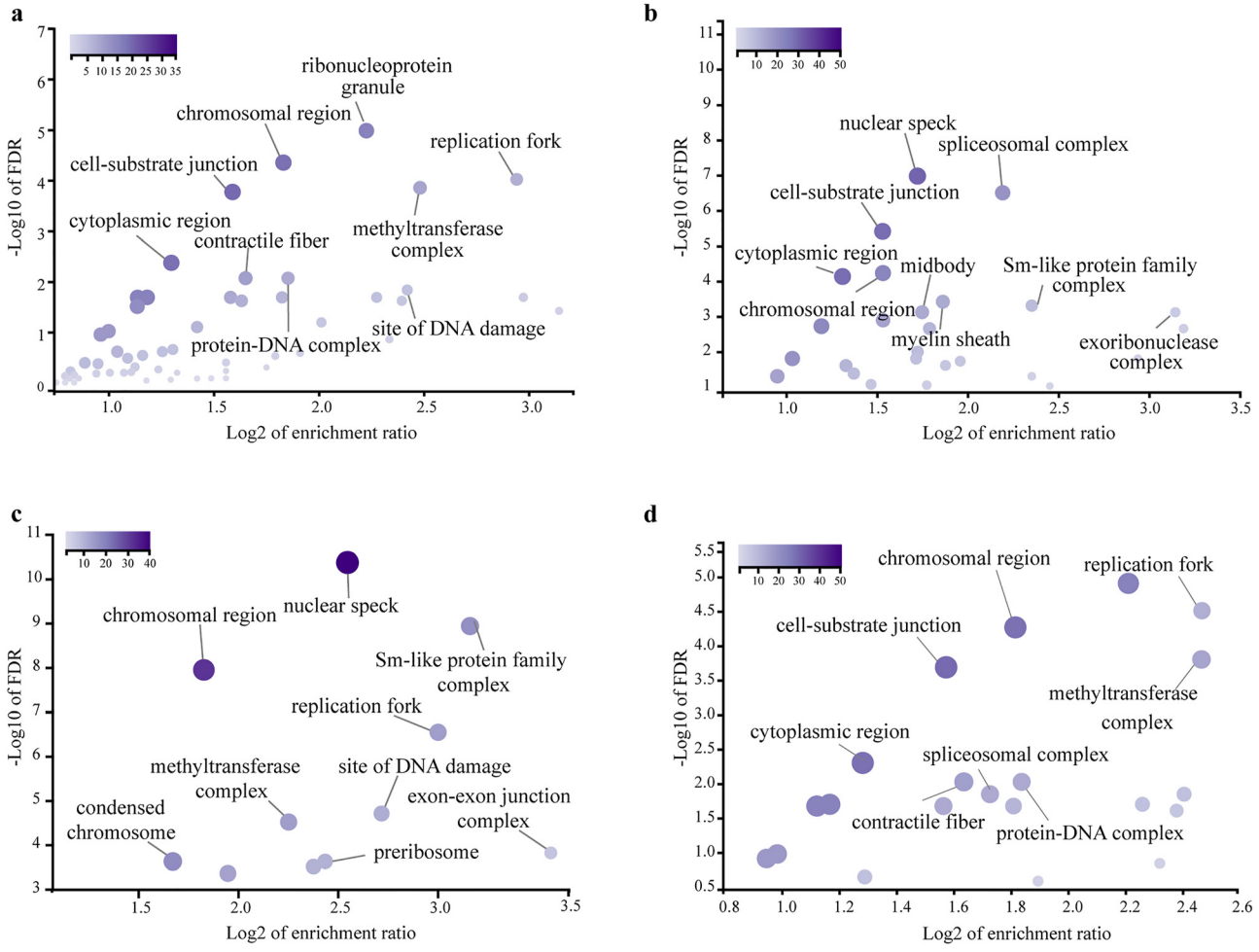

Figure 5: Subcellular localization of MST1-interacting proteins in different cell death. Subcellular localization of MST1-interacting proteins in (a) the common module, (b) apoptosis, (c) autophagy, and (d) pyroptosis. The WebGestalt analysis software was employed to generate volcano plots for visualization ($p<0.05$ for each GO term).

localization to methyltransferase, contractile fibers, and protein-DNA complexes.

Discussion

MST1, a crucial stress-regulated protein, engages in various cellular processes through interactions influencing protein homeostasis and metabolic function. Despite its significance, no prior study has comprehensively captured and analyzed MST1's interaction partners, particularly in distinct cell death scenarios. Acknowledging the importance of subcellular complexity and spatial context in protein function, we employed the APEX2 labeling method and IP-MS to identify all proximity partners of MST1 in ESCC cells under diverse cell death conditions. There are two major limitations in this study that could be addressed in future research. First, it is imperative to acknowledge that this study primarily focuses on a specific temporal snapshot during the occurrence of cell death, thus not comprehensively representing the entirety of the regulatory dynamics governing the process. Second, the molecular pathway of the significantly differential binding protein of MST1 has not been verified, and our results provide the insights for future study on the molecular mechanism of MST1 regulating different cell death.

Previous studies have classified MST1 as a pro-apoptotic kinase [39]. Our research revealed that mitosis-related proteins binding significantly increased in drug-induced apoptosis, such as SHCBP1, KIF23 and ANLN which have been reported to promote cell proliferation [40, 41]. This suggested a potential yet unconfirmed role of MST1 in regulating mitosis during drug-induced apoptosis. Additionally, the interaction between MST1 and MST2, another pro-apoptotic kinase in the STE family diminished. It has been observed that MST1 and MST2 can form heterodimers, and the enzymatic activity of MST1/MST2 heterodimers is notably reduced [42]. Due to the limited research in this domain, further investigation is needed to elucidate the impact of this change on cell death.

Autophagy has been reported to influence the activity of the DNA repair machinery and positively regulates DNA damage recognition by nucleotide excision repair [43, 44]. In the autophagy model, the binding between CBX8 and YTHDC1 with MST1 significantly increased. CBX8 is highly expressed in ESCC tissue [45] and participates in DNA repair, while YTHDC1 can promote autophagy by targeting the autophagic adaptor SQSTM1 [46]. Cytoskeletal dynamics regulate the condensation of p62 bodies containing SQSTM1 [47], while our findings indicate that the decreased binding proteins in autophagy are mainly associated with cytoskeletal proteins. Thus, in rapamycin-induced autophagy, MST1 primarily participates in DNA repair and cytoskeleton regulation. Considering these findings, MST1 is likely to further promote cellular autophagy in drug-induced autophagy, contrary to its previously reported inhibitory role in autophagy and we speculate that this discrepancy might reflect cellular adaptation to drug stimuli.

Activation of NLRP3 promotes the cleavage of caspase-1, thereby facilitating pyroptosis [45]. In the pyroptosis model, the interaction between LRRFIP2 and FLII with MST1 was significantly enhanced, while LRRFIP2 negatively regulates NLRP3 inflammasome activation by promoting FLII-mediated caspase-1 inhibition [48]. This suggests a potential mechanism: in TSA-induced pyroptosis, MST1 enhances the binding and activation of LRRFIP2 and FLII, thus inhibiting pyroptosis.

These analytical findings suggest that patients with elevated MST1 expression may be more prone to developing cisplatin resistance due to its increased interaction with mitotic-related proteins during cisplatin-induced apoptosis, and they may also exhibit reduced sensitivity to pyroptosis-inducing drugs. Moreover, MST1's beneficial effect on DNA repair may influence the well-established chemotherapy resistance mediated by autophagy in cancer cells. Importantly, MST1 interactomes consistently exhibit resistance to regulated cell death, and their molecular functions are linked to chromatin remodeling in three drug-induced cell death models.

In conclusion, this study offers a preliminary understanding and abundant resources of MST1 interactomes and potential mechanisms for regulating cell death. Subsequent drug sensitivity and animal experiments will validate the impact of MST1 interactions across different cellular contexts.

Acknowledgments: We express gratitude to Shenzhen Bay Laboratory for providing facilities and technical support. We are also appreciative of the valuable comments and discussions contributed by all members of our laboratory.
Research ethics: Not applicable.
Informed consent: Not applicable.
Competing interests: Authors state no conflict of interest.
Research funding: This work was supported by the funds of Guangdong Basic and Applied Basic Research Foundation (2019B030302012), the National Key R&D Program of China (2021YFC2501001, 2022YFC3401002), Shenzhen Medical Research Funds (C2303002), the National Natural Science Foundation of China (82341024, 82172930, 82203286), the Major Program of Shenzhen Bay Laboratory (S201101004) and China Postdoctoral Science Foundation (BX20220214).
Author contributions: The study was conceived and supervised by Y.P.C. and W.M.Z. All experiments and analysis were conducted by L.Z. with assistance from M.W.G., Y.G.W., H.J.L., Y.Z., Q.Q.S. and S.S.B. The MST1 expression analysis of

ESCC patients was conducted by X.H.Z. The manuscript was written by L.Z. and was revised by Y.P.C. and W.M.Z. All the authors have read and approved the manuscript.

Data Availability: Data available on request from the correspondence author.

References

1. Abnet CC, Arnold M, Wei WQ. Epidemiology of esophageal squamous cell carcinoma. Gastroenterology 2018;154:360–73.
2. Sung H, Ferlay J, Siegel RL, Laversanne M, Soerjomataram I, Jemal A, et al. Global cancer statistics 2020: GLOBOCAN estimates of incidence and mortality worldwide for 36 cancers in 185 countries. CA Cancer J Clin 2021;71:209–49.
3. Cui J, Zhou Z, Yang H, Jiao F, Li N, Gao Y, et al. MST1 suppresses pancreatic cancer progression via ROS-induced pyroptosis. Mol Cancer Res 2019;17:1316–25.
4. Wilkinson DS, Jariwala JS, Anderson E, Mitra K, Meisenhelder J, Chang JT, et al. Phosphorylation of LC3 by the Hippo kinases STK3/STK4 is essential for autophagy. Mol Cell 2015;57:55–68.
5. Rawat SJ, Chernoff J. Regulation of mammalian Ste20 (Mst) kinases. Trends Biochem Sci 2015;40:149–56.
6. Klionsky DJ, Abdel-Aziz AK, Abdelfatah S, Abdellatif M, Abdoli A, Abel S, et al. Guidelines for the use and interpretation of assays for monitoring autophagy (4th edition)[1]. Autophagy 2021;17:1–382.
7. Zeng Q, Hong W. The emerging role of the Hippo pathway in cell contact inhibition, organ size control, and cancer development in mammals. Cancer Cell 2008;13:188–92.
8. Yu FX, Zhao B, Guan KL. Hippo pathway in organ size control, tissue homeostasis, and cancer. Cell 2015;163:811–28.
9. Harvey KF, Zhang X, Thomas DM. The Hippo pathway and human cancer. Nat Rev Cancer 2013;13:246–57.
10. Johnson R, Halder G. The two faces of Hippo: targeting the Hippo pathway for regenerative medicine and cancer treatment. Nat Rev Drug Discov 2014;13:63–79.
11. Zhao B, Wei X, Li W, Udan RS, Yang Q, Kim J, et al. Inactivation of YAP oncoprotein by the Hippo pathway is involved in cell contact inhibition and tissue growth control. Gene Dev 2007;21:2747–61.
12. Green DR, Llambi F. Cell death signaling. Cold Spring Harbor Perspect Biol 2015;7:a006080.
13. Gentilin E. New advancements in cisplatin-based treatments. Int J Mol Sci 2023;24:5920.
14. Lee E, Han AR, Nam B, Kim YR, Jin CH, Kim JB, et al. Moscatilin induces apoptosis in human head and neck squamous cell carcinoma cells via JNK signaling pathway. Molecules 2020;25:901.
15. Green DR. Caspase activation and inhibition. Cold Spring Harbor Perspect Biol 2022;14:a041020.
16. Chen X, He WT, Hu L, Li J, Fang Y, Wang X, et al. Pyroptosis is driven by non-selective gasdermin-D pore and its morphology is different from MLKL channel-mediated necroptosis. Cell Res 2016;26:1007–20.
17. Samanta S, Zhou Z, Rajasingh S, Panda A, Sampath V, Rajasingh J. DNMT and HDAC inhibitors together abrogate endotoxemia mediated macrophage death by STAT3-JMJD3 signaling. Int J Biochem Cell Biol 2018;102:117–27.
18. Ahrens TD, Timme S, Hoeppner J, Ostendorp J, Hembach S, Follo M, et al. Selective inhibition of esophageal cancer cells by combination of HDAC inhibitors and azacytidine. Epigenetics 2015;10:431–45.
19. Zhu Y, Yuan T, Zhang Y, Shi J, Bai L, Duan X, et al. AR-42: a pan-HDAC inhibitor with antitumor and antiangiogenic activities in esophageal squamous cell carcinoma. Drug Des Dev Ther 2019;13:4321–30.
20. Wang Y, Gao W, Shi X, Ding J, Liu W, He H, et al. Chemotherapy drugs induce pyroptosis through caspase-3 cleavage of a gasdermin. Nature 2017;547:99–103.
21. White E, DiPaola RS. The double-edged sword of autophagy modulation in cancer. Clin Cancer Res 2009;15:5308–16.
22. Levy JMM, Towers CG, Thorburn A. Targeting autophagy in cancer. Nat Rev Cancer 2017;17:528–42.
23. Hou G, Zhang Q, Wang L, Liu M, Wang J, Xue L. mTOR inhibitor rapamycin alone or combined with cisplatin inhibits growth of esophageal squamous cell carcinoma in nude mice. Cancer Lett 2010;290:248–54.
24. Lam SS, Martell JD, Kamer KJ, Deerinck TJ, Ellisman MH, Mootha VK, et al. Directed evolution of APEX2 for electron microscopy and proximity labeling. Nat Methods 2015;12:51–4.
25. Honda R, Körner R, Nigg EA. Exploring the functional interactions between Aurora B, INCENP, and survivin in mitosis. Mol Biol Cell 2003;14:3325–41.
26. Kiyomitsu T, Cheeseman IM. Cortical dynein and asymmetric membrane elongation coordinately position the spindle in anaphase. Cell 2013;154:391–402.
27. Zhao W-M, Fang G. Anillin is a substrate of anaphase-promoting complex/cyclosome (APC/C) that controls spatial contractility of myosin during late cytokinesis. J Biol Chem 2005;280:33516–24.
28. Makyio H, Ohgi M, Takei T, Takahashi S, Takatsu H, Katoh Y, et al. Structural basis for Arf6-MKLP1 complex formation on the Flemming body responsible for cytokinesis. EMBO J 2012;31:2590–603.
29. Shi W, Zhang G, Ma Z, Li L, Liu M, Qin L, et al. Hyperactivation of HER2-SHCBP1-PLK1 axis promotes tumor cell mitosis and impairs trastuzumab sensitivity to gastric cancer. Nat Commun 2021;12:2812.
30. Chen Y, Yang L, Qin Y, Liu S, Qiao Y, Wan X, et al. Effects of differential distributed-JUP on the malignancy of gastric cancer. J Adv Res 2021;28:195–208.
31. Qu J, Zhu L, Zhou Z, Chen P, Liu S, Locy ML, et al. Reversing mechanoinductive DSP expression by CRISPR/dCas9-mediated epigenome editing. Am J Respir Crit Care Med 2018;198:599–609.
32. Bottini A, Wu DJ, Ai R, Le Roux M, Bartok B, Bombardieri M, et al. PTPN14 phosphatase and YAP promote TGFbeta signalling in rheumatoid synoviocytes. Ann Rheum Dis 2019;78:600–9.
33. Oza J, Ganguly B, Kulkarni A, Ginjala V, Yao M, Ganesan S. A novel role of chromodomain protein CBX8 in DNA damage response. J Biol Chem 2017;292:761.
34. Okuwaki M, Sumi A, Hisaoka M, Saotome-Nakamura A, Akashi S, Nishimura Y, et al. Function of homo- and hetero-oligomers of human nucleoplasmin/nucleophosmin family proteins NPM1, NPM2 and NPM3 during sperm chromatin remodeling. Nucleic Acids Res 2012;40:4861–78.
35. Wang M, Dai M, Wang D, Tang T, Xiong F, Xiang B, et al. The long noncoding RNA AATBC promotes breast cancer migration and invasion by interacting with YBX1 and activating the YAP1/Hippo signaling pathway. Cancer Lett 2021;512:60–72.
36. Hermeking H, Benzinger A. 14-3-3 proteins in cell cycle regulation. Semin Cancer Biol 2006;16:183–92.
37. Fäßler F, Dimchev G, Hodirnau V-V, Wan W, Schur FKM. Cryo-electron tomography structure of Arp2/3 complex in cells reveals new insights into the branch junction. Nat Commun 2020;11:6437.

38. Lim J, Ha M, Chang H, Kwon SC, Simanshu DK, Patel DJ, et al. Uridylation by TUT4 and TUT7 marks mRNA for degradation. Cell 2014;159:1365–76.
39. Yin Y, Tan M, Han L, Zhang L, Zhang Y, Zhang J, et al. The Hippo kinases MST1/2 in cardiovascular and metabolic diseases: a promising therapeutic target option for pharmacotherapy. Acta Pharm Sin B 2023;13:1956–75.
40. Saito Y, Yin D, Kubota N, Wang X, Filliol A, Remotti H, et al. A therapeutically targetable TAZ-TEAD2 pathway drives the growth of hepatocellular carcinoma via ANLN and KIF23. Gastroenterology 2023; 164:1279–92.
41. Xu N, Wu Y-P, Yin H-B, Chen S-H, Li X-D, Xue X-Y, et al. SHCBP1 promotes tumor cell proliferation, migration, and invasion, and is associated with poor prostate cancer prognosis. J Cancer Res Clin Oncol 2020;146: 1953–69.
42. Rawat SJ, Araiza-Olivera D, Arias-Romero LE, Villamar-Cruz O, Prudnikova TY, Roder H, et al. H-Ras inhibits the Hippo pathway by promoting mst1/Mst2 heterodimerization. Curr Biol 2016;26: 1556–63.
43. Gomes LR, Menck CFM, Leandro GS. Autophagy roles in the modulation of DNA repair pathways. Int J Mol Sci 2017;18:2351.
44. Qiang L, Zhao B, Shah P, Sample A, Yang S, He YY. Autophagy positively regulates DNA damage recognition by nucleotide excision repair. Autophagy 2016;12:357–68.
45. Zhang L, Zhou Y, Cheng C, Cui H, Cheng L, Kong P, et al. Genomic analyses reveal mutational signatures and frequently altered genes in esophageal squamous cell carcinoma. Am J Hum Genet 2015;96:597–611.
46. Liang D, Lin WJ, Ren M, Qiu J, Yang C, Wang X, et al. m(6)A reader YTHDC1 modulates autophagy by targeting SQSTM1 in diabetic skin. Autophagy 2022;18:1318–37.
47. Feng X, Du W, Ding M, Zhao W, Xirefu X, Ma M, et al. Myosin 1D and the branched actin network control the condensation of p62 bodies. Cell Res 2022;32:659–69.
48. Jin J, Yu Q, Han C, Hu X, Xu S, Wang Q, et al. LRRFIP2 negatively regulates NLRP3 inflammasome activation in macrophages by promoting flightless-I-mediated caspase-1 inhibition. Nat Commun 2013;4:2075.
49. Liao Y, Wang J, Jaehnig EJ, Shi Z, Zhang B. WebGestalt 2019: gene set analysis toolkit with revamped UIs and APIs. Nucleic Acids Res 2019;47: W199–205.
50. Bindea G, Mlecnik B, Hackl H, Charoentong P, Tosolini M, Kirilovsky A, et al. ClueGO: a cytoscape plug-in to decipher functionally grouped gene ontology and pathway annotation networks. Bioinformatics 2009;25:1091–3.

Supplementary Material: This article contains supplementary material (https://doi.org/10.1515/mr-2024-0031).